JAEA-Review
2008-013

JAEA-Review

Electrons in Condensed Media

Asokendu MOZUMDER*, Akinari YOKOYA, Yosuke KATSUMURA and Yoshihiko HATANO

Advanced Science Research Center

June 2008

Japan Atomic Energy Agency

日本原子力研究開発機構

独立行政法人日本原子力研究開発機構　研究技術情報部　研究技術情報課
〒319-1195　茨城県那珂郡東海村白方白根 2 番地 4
電話 029-282-6387, Fax 029-282-5920, E-mail:ird-support@jaea.go.jp

JAEA-Review 2008-013

Electrons in Condensed Media

Asokendu MOZUMDER*, Akinari YOKOYA, Yosuke KATSUMURA
and Yoshihiko HATANO

Advanced Science Research Center, Japan Atomic Energy Agency
Tokai-mura, Naka-gun, Ibaraki-ken

(Received January 29, 2008)

This document is a summary of the lectures or seminar talks by A.Mozumder and his discussion/information exchanges with Y.Hatano, A.Yokoya, and Y.Katsumura. A.Mozumder is an invited fellow of the JSPS Invitation Fellowship Program for Research in Japan (Short-Term) with the host Y.Hatano, and stays in Japan mainly at Advanced Science Research Center (ASRC) of JAEA for 52 days starting from September 27 through November 17, 2007. The research in this program is entitled "Charged Particle and Photon Interactions with Matter", from which the authors give the title of this document one of the most important reactive species commonly produced in matter from these interactions. This document contains the annotated materials presented at ten seminars given by A.Mozumder during his stay in Japan in this program at JAEA (Tokai and Takasaki) and also at various universities and research institutes, including invited lectures at the International Symposium of ASR2007 held in Tokai and the Annual Discussion Meeting of Radiation Chemistry held in Kyoto. Some information exchanged frequently at informal discussion with the group of Y. Katsumura and A. Yokoya at ASRC are also incorporated. The following write-up is divided into five sections, according to the subject matters discussed. These are respectively as follows. (1) Early Stages in the Radiolysis of Liquid Water: Consequences of Excitation, Ionization and Dissociative Electron Attachment. (2) Differential Oscillator Distribution (DOSD) in Liquid Water and G-values of Excitation and of Ionization. (3) Quasi-Ballistic Model of Electron Mobility in Liquid Hydrocarbons including Thermodynamics, Scavenging and Relation Between Free-Ion Yield and Mobility. (4) Electron Localization: The Anderson Model. And (5) Free-ion Yield in Liquefied Rare Gases: A new Theoretical Model.

This work was performed by (JSPS Invitation Fellowship Program for Research in Japan (Short Term) Program.

* University of Notre Dame

Keywords: Electron Mobility, Condensed Media, Radiolysis, Liquid Water, Excitation and Ionization, Differential Oscillator Distribution, G-values, Free-Ion Yield, Quasi-Ballistic Model, The Anderson Model

凝縮相における電子の振舞い

日本原子力研究開発機構 先端基礎研究センター
Asokendu　MOZUMDER*、 横谷　明徳、勝村　庸介、簇野　嘉彦

(2008 年 1 月 29 日　受理)

このＲeview は、下記研究課題のうち特に標記の課題について、A.Mozumder によるセミナー等の研究集会における講演と横谷明徳、勝村庸介、簇野嘉彦等と行った情報・意見交換の内容をまとめたものである。A.Mozumder は日本学術振興会外国人招へい研究者（短期）（受入研究者：簇野嘉彦、期間：本年９月 27 日から 11 月 17 日まで、研究課題：「荷電粒子およびフォトンと物質との相互作用」）として日本原子力研究開発機構先端基礎研究センターに招へいされた。標記の課題は、上記の相互作用のいずれの場合においても共通に生成される反応分子種のうちから最も重要なものとして電子を選んで、特に凝縮相におけるその振る舞いについて述べたもので、A.Mozumder が行った本機構（東海および高崎地区）および国内の諸大学、研究機関でのセミナー等の講演、本センターが主催した国際シンポジウム ASR2007 および放射線化学討論会（京都）での招待講演、本センターの勝村・横谷グループと頻繁に行った情報・意見交換の内容をまとめたものである。この Review は、研究内容に応じて次の 6 章から構成される。(1) 水の液相放射線分解の初期過程：励起、イオン化及び解離性電子付着。(2) 液相の水の微分振動子強度分布と励起及びイオン化の G 値。(3) 液体炭化水素中における電子移動度に関する熱力学を考慮した Quasi-Ballistic モデル、スキャベンジング及び自由イオン収率と 移動度の関連について。(4) 電子の局在化 ：アンダーソンモデル。(5) 液体希ガス中における自由イオン収率―新規な理論モデル。(6) まとめ。

本報告書は、(日本学術振興会外国人招へい(短期)受入れ研究者の受入れにより実施した研究成果に関するものである。

原子力科学研究所（駐在）：〒319-1195　茨城県那珂郡東海村白方白根 2-4
＊　米国ノートルダム大学

This is a blank page.

Contents

1. Early stage in the radiolysis of liquid water ---------- 1

2. Differential oscillator distribution (DOSD) in liquid water and the G-values of excitation and of ionization ---------- 7

3. The quasi-ballistic model of electron mobility in liquid hydrocarbons ---------- 11

4. Electron localization in hydrocarbon liquids: The Anderson model ---------- 24

5. Free-ion yield in liquefied rare gases: A new theoretical model ---------- 33

6. Summary ---------- 37

目　次

1. 液相の水の放射線分解の初期過程：励起、イオン化及び解離性電子付着 ---------- 1

2. 液相の水の微分振動子強度分布と励起及びイオン化の G 値 ---------- 7

3. 液体炭化水素中における電子移動度に関する熱力学を考慮した Quasi-Ballistic モデル ---------- 11

4. 電子の局在化 ：アンダーソンモデル ---------- 24

5. 液体希ガス中における自由イオン収率：新規な理論モデル ---------- 33

6. まとめ ---------- 37

This is a blank page.

1. Early stage in the radiolysis of liquid water

Fig. 1 describes our latest understanding about the initial stages of the radiolysis of liquid water following energy deposition in electronic form. Usually, the major channels are ionization, followed by ion-molecule reaction with the positive ion giving $H_3O^+ and OH$ and also production of the electron which eventually solvates.

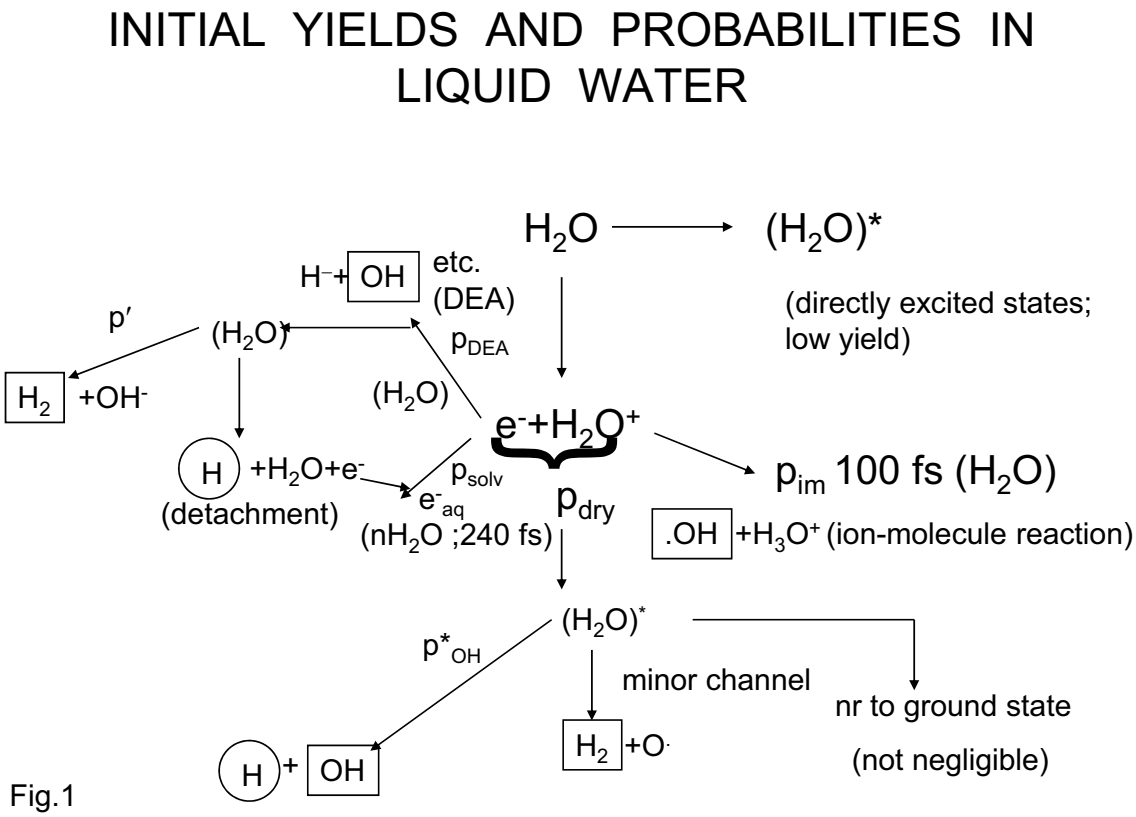

Fig.1

The minor channel is the production of excited states either directly, or as a result of dry electron-positive ion recombination. These excited states, when produced, can give a small yield of $HandOH$ or of $H_2 and O$. Before solvation, the ejected electron undergoes moderation in energy by various intramolecular processes. When its energy is in the interval ~5-15 eV, it can undergo a dissociative electron attachment (DEA) reaction with a water molecule producing mainly $H^- and OH$. The negative ion can generate an H-atom by a detachment process. Infrequently, it can also extract a proton to give 'unscavengable' H_2. In our opinion, DEA is the main channel for the primary H-atom production.

Equations for Initial Yields

$$G^0(e^-_{aq}) = G^0_{ion}[(p_{sol} + p_{DEA}(1-p')] \quad (2.1)$$

$$G^0(H_2) = G^0_{ion}[p_{dry}(1-p^*_{OH}-p_{nr}) + p_{DEA}p'] + G^0_{ex}(1-p^*_{OH}-p_{nr}) \quad (2.2)$$

$$\mathrm{G}^0(H) = G^0_{ion}[p_{DEA}(1-p') + p_{dry}p^*_{OH}] + G^0_{ex}p^*_{OH} \quad (2.3)$$

$$\mathrm{G}^0(OH) = G^0_{ion}[p_{im} + p_{dry}p^*_{OH} + p_{DEA}] + G^0_{ex}p^*_{OH} \quad (2.4)$$

$$\mathrm{G}^0(H_3O^+) = G^0(e^-_{aq}) + G^0(OH^-) = G^0_{ion}p_{im} \text{ [from (1.1) and (1.2)]} \quad (2.5)$$

$$\mathrm{G}^0(OH^-) = G^0_{ion}p_{DEA}p' \quad (2.6)$$

$$\mathrm{G}^0(O) = G^0_{ion}[p_{dry}(1-p^*_{OH}-p_{nr})] + G^0_{ex}(1-p^*_{OH}-p_{nr}) \quad (2.7)$$

Fig.2

Fig.2 gives the equations for the various initial yields, obtained in consistency with the mechanism described in Fig.1.For example, eq.(1) is for e^-_{aq} and eq.(4) for OH. These equations are nothing but a collection of various processes by which a particular entity would be formed.

Estimated Initial Yields

Taking $p_{dry} = 0.07$,

$p_{DEA} = 0.15$,

$p' = 0.2$,

one gets $p_{sol} = 0.78$,

$p_{im} = 0.93$.

Using $\mathrm{G}^0(e^-_{aq}) = 4.0$,

one gets $G^0_{ion} = 4.44$ and successively,

$G^0(H_2) = 0.16$; $G^0(H) = 0.75$; $G^0(OH) = 4.99$; $G^0(H_3O^+) = 4.13$

$G^0(OH^-)0.13$ and $G^0(O) = 0.024$

A small yield (0.13) is needed for charge balance

Fig.3

Fig. 3 shows the estimated G-values of the primary species. These have been collected mainly by extrapolation of measured G-values at longer times, where available, with the assistance of theoretical evaluation. Only the probability of dissociative electron attachment, $p_{DEA} = 0.15$, before the electron thermalizes, was computed by Monte Carlo simulation using the solid phase cross-section data (Pimblott, unpublished). Notice that a small yield of $G^0(OH^-) = 0.13$ is needed for charge balance. The estimated yields of $G^0(e^-_{aq}) = 4.0, G^0(OH) = 4.99, G^0(H_2) = 0.16 and G^0(H) = 0.75$ are in good agreement with experimental values. These imply the total ionization yield in liquid water to be G^0_{ion}=4.44.

Initial Yields in Liquid Water

(1) Branching Ratio $H^- + H_2O \rightarrow H_2 + OH^-$;
or $\rightarrow H + H_2O + e^-$
depends on energy (5-15 eV)

(2) Total initial yield G^0_{ion} *(various)*.
$G^0_{ex} = G^d_{ex} + G^{DEA}_{ex}$

(3) Total OH yield = ion-mol reaction +
direct reaction + DEA reaction.

(4) Initial H_2 yield ~ 1/3 the observed yield.

Fig.4

Fig.4 illustrates the branching ratio of the reaction of $H^- with H_2O$, giving either a primary H_2 molecule, or simply a detachment forming an H-atom. The next two items give the different ways in which H and OH may be formed. The last item is a requirement of the diffusion model of Schwarz at low-LET.

Quantum Efficiencies of Ionization and Dissociation

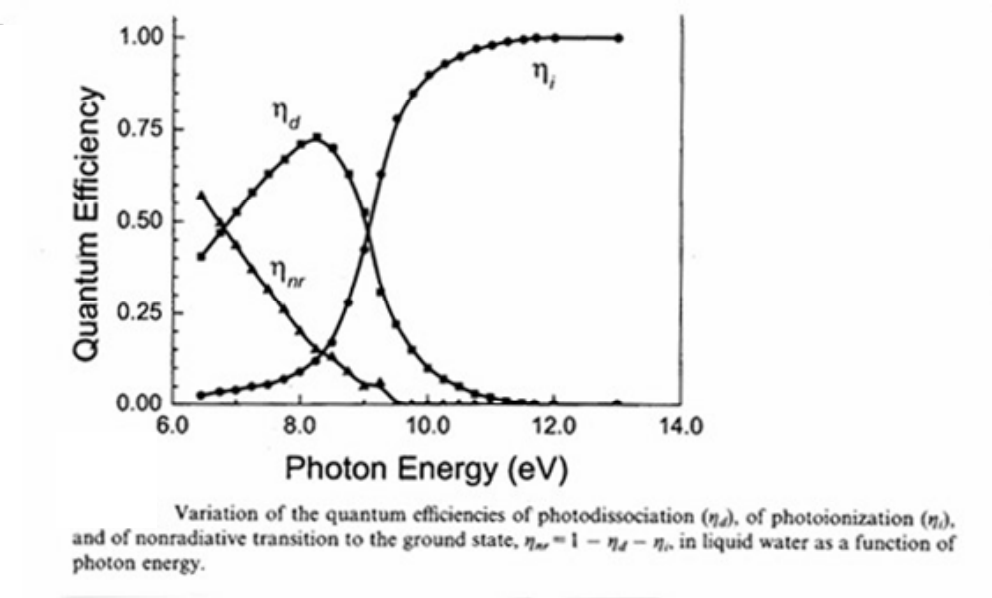

Variation of the quantum efficiencies of photodissociation (η_d), of photoionization (η_i), and of nonradiative transition to the ground state, $\eta_{nr} = 1 - \eta_d - \eta_i$, in liquid water as a function of photon energy.

Fig.5

Fig.5 collects the quantum efficiencies of ionization and excitation in liquid water that have been measured over the decades. The earlier data were obtained in the low energy regime, while later experiments give more precise data obtained with 1- or 2-photon laser work, up to ~10 eV and beyond. The sum of these two efficiencies falls short of unity and the difference must be accounted for by non-radiative transition to the ground state. This important point was missed in many earlier theoretical work. The large difference between calculated and observed dissociation yields then required the postulation of a cage effect, which has never been established in liquid water. The existence of a significant probability of non-radiative transition to the ground state obviates the necessity of cage recombination. Incidentally, if we define the ionization potential of liquid water as the energy needed to reach unit efficiency of ionization, and attribute the process to the transition to the lowest conduction state in the liquid, then we find no evidence of superexcited states in liquid water which should be an important observation. So-defined ionization potential in liquid water is found to be 11.7 ± 0.2 eV.

Early Photochemical Results

$$H_2O + h\nu \rightarrow H + OH \qquad \text{(I)}$$
$$\rightarrow H_2 + O \qquad \text{(II)}$$

McNesby at al. (1962), I : II = 3 : 1 at 10.3 eV
Black and Porter (1962), = 9 : 1 for $h\nu > 6.52$ eV
Steif et al. (1975), = 0.99 : 0.01 for $h\nu = 6.70 - 8.54$ eV
= 0.89 : 0.11 for $h\nu = 8.54 - 11.80$ eV

$$(H_2O)_{aq} \xrightarrow{h\nu} (H_2O)^{**}_{aq} \rightarrow e^-_{aq} + OH + H_3O^+_{aq}$$

Fig.6

Some early photochemical results are shown in fig.6. Apparently, the direct formation of the hydrated electron was envisaged, even though probably without an understanding of the mechanism. It is now known that these low-energy processes are due neither to direct ionization, nor to auto-ionization, but due to optical charge transfer, or photo-induced electron transfer. Fig. 7 shows the fate of neutral excitation in liquid water according to Bartels and Crowell. Most of the excited states are converted to ionization by interaction with nearby water molecules. What is absent here is the crossing with highly excited vibrational state of the ground electronic state, by which a non-radiative transition to the ground state may be affected.

Fate of Excitation in Liquid Water

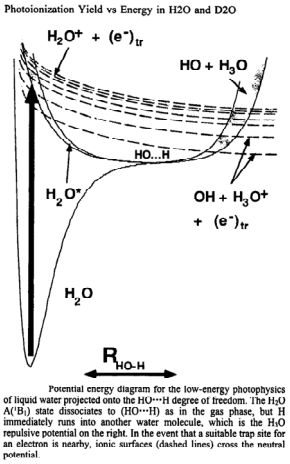

Fig.7

Cited from David M. Bartels and Robert A. Crowell (2000), Photoionization Yield vs. Energy in H_2O and D_2O. J. Phys. Chem. A 104, 3849–3355

Dissociative Electron Attachment in Liquid Water

- Direct dissociation yield in liquid water is very low, G~0.01 or less.
- Monte Carlo simulation (Pimblott) indicates a probability ~20% for electrons in energy interval 5-15 eV to undergo DEA, giving an yield ~ 0.2 x 4.0 (ionization yield) = 0.8.
- DEA mainly produces carries
- most of the excess energy. The hot invariably loses the electron by collision.
- Net effect of DEA in liquid water is dissociation of an water molecule into separated by a few water molecules and an electron degraded in energy.

Fig.8

Fig. 8 gives some details of DEA in liquid water. The direct production of H and OH from an excited state in unlikely in liquid water, partly because of small oscillator strength of those excitations, and partly because of strong non-radiative transition at low energy and high probability of going over to ionization at higher energies. Fig. 9 gives our view on the ionization potential in liquid water and evaluates it to be 11.7 ± 0.2 eV (vide supra).

Ionization Potential of Liquid Water

- Lower energy processes giving the hydrated electron are due to neither direct nor auto-ionization, but due to optical charge transfer or photo-induced electron transfer (Sander et al.).
- Concerted proton-coupled electron transfer operates at higher energy (Keszei and Jay-Gerin).
- Mozumder defines I.P. in liquid water as the minimum energy needed to generate a quasi-free electron in the band gap and evaluates it as 11.7 + or - 0.2 eV.
- Based on ionization efficiency, existence of superexcited states is denied in liquid water.

Fig.9

2. Differential oscillator distribution (DOSD) in liquid water and the G-values of excitation and of ionization

Figs. 10-17 summarize our calculations for the primary (first collision) yields of ionization and excitation in liquid water, starting from experimental measurements of DOSD. Some heuristic procedure, based on energy balance, has been used to get at the total ionization yield, which however cannot be done for excitation.

UV-Reflectance and DOSD

$$\phi(E) = (E/\pi)P\int_0^\infty \frac{\ln R(E')}{(E')^2 - E^2}dE'$$

$$n = (1-R)/(1+R-2R^{1/2}\cos\phi); k = -2R^{1/2}\sin\phi/(1+R-2R^{1/2}\cos\phi)$$

$$\varepsilon_1 = n^2 - k^2; \varepsilon_2 = 2nk$$

$$\mathrm{Im}(-1/\varepsilon) = \varepsilon_2/(\varepsilon_1^2+\varepsilon_2^2) = (h^2e^2N/2m)f(E)/E;\ \mathrm{DOSD} = f(E)$$

Fig.10

Condensed Phase Dielectric Function

Condensed phase relection data gives dielctric function

$$\varepsilon = \varepsilon_1 + i\varepsilon_2;\ \mathrm{Im}(-1/\varepsilon) = \varepsilon_2/(\varepsilon_1^2+\varepsilon_2^2)$$

$$\mathrm{Im}(-1/\varepsilon) = (h^2e^2NZ/2m)f'(E)/E$$

$f'(E)$ is the differential oscillator strength at energy E.

Fig.11

Oscillator Strength (DOSD) in Water

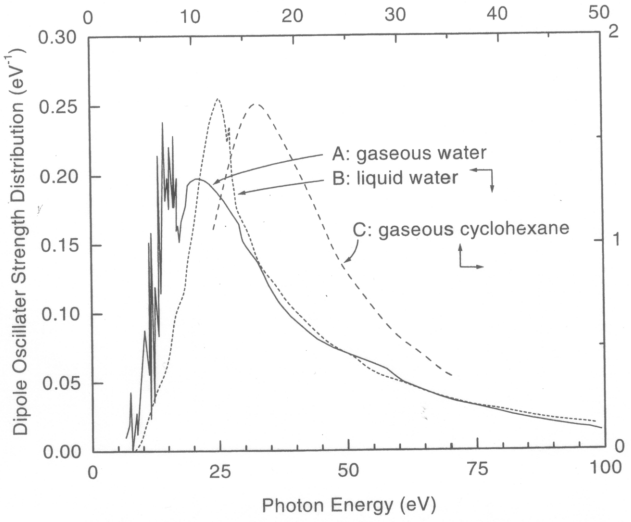

Dipole oscillator strength distribution in gaseous water [29, curve, A], in liquid water [31, curve, B] and in gaseous cyclohexane [32, curve, C]. Data in liquid water are obtained from an analysis of UV-reflectance and that in cyclohexane, from synchrotron–UV absorption. The Thomas–Kuhn sum rule is satisfied approximately in each case.

Fig.12

Optical and Excitation Spectrum in Liquid Water

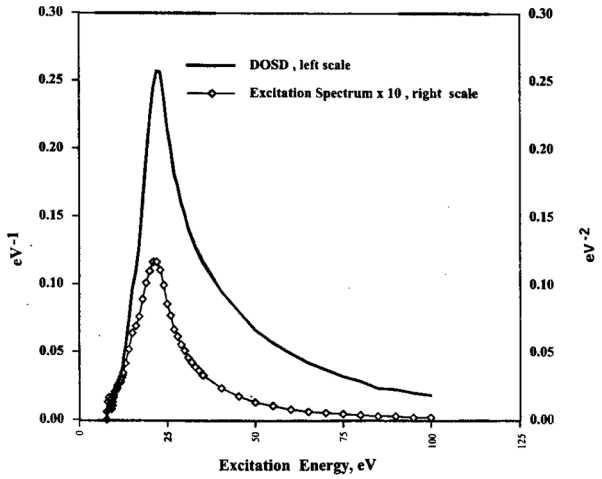

Dipole oscillator strength distribution (DOSD, the optical spectrum) and the excitation spectrum of liquid water up to 100 eV.[5a] Extension of the excitation spectrum to the maximum transferable energy is used to calculate the yields due to the primary irradiation.

Fig.13

Fig. 10 shows the usual relationship between UV-reflectance and the complex refractive index, from which the complex dielectric constant is easily derived. It is the imaginary part of the reciprocal of the complex dielectric constant that is directly proportional to the DOSD, as given in Fig.11, which is particularly useful in the condensed media. Note that, using only the UV-data requires long extrapolation which is now obviated by the use of synchrotron radiation absorption measurement. So-obtained DOSD in water, in both gaseous and condensed phases of water are, shown in Fig. 12 and compared with that of gaseous cyclohexane obtained by Hatano et al. Comparison between gaseous and condensed water reveals a loss of structure and an upshift in energy of the DOSD in the condensed phases. This has important consequence on the very low yield of excitation in liquid water (vide infra). Fig. 13 compares the optical and excitation spectra of liquid water. They are similar, except for an energy denominator for the excitation spectrum.

Cross-Section for Energy Loss [Born-Bethe]

$$d\sigma/d\varepsilon = \kappa[\{f'(\varepsilon)/\varepsilon\}\ln(\varepsilon_m/\varepsilon) + n(\varepsilon)/\varepsilon^2]; \kappa = 2\pi z^2 e^4/mv^2; n(\varepsilon) = \int^{\varepsilon} f'(\varepsilon)d\varepsilon.$$

glancing head-on

$$S = -(dE/dx) = 2\kappa ZN\ln(\varepsilon_m/I)$$

$$Z = \int^{\varepsilon_m} f'(\varepsilon)d\varepsilon \quad \text{(Thomas-Kuhn Sum Rule)}$$

$$Z\ln I = \int^{\varepsilon_m} f'(\varepsilon)\ln\varepsilon d\varepsilon; \varepsilon_m = 0.583mv^2.$$

$$G^P = [100/2Z\ln(\varepsilon_m/I)]\int_{\varepsilon_0}^{\varepsilon_m}\eta[\frac{f'(\varepsilon)}{\varepsilon}\ln(\varepsilon_m/\varepsilon) + n(\varepsilon)/\varepsilon^2]d\varepsilon; \eta = \eta_i \text{ or } \eta_d.$$

Fig.14

Estimate of Total Ionization Yield

- Example : Primary electron of energy 50 KeV. Ionization yield produced by the primary electron is divided into four categories according to energy loss:
- (1) 0.045 for $\varepsilon_0 \le \varepsilon \le \varepsilon_1 = I.P. = 11.7\ \mathrm{eV}$
- (2) 0.618 for $\varepsilon_1 \le \varepsilon \le 35\ \mathrm{eV}$
- (3) 0.178 for $35\mathrm{eV} \le \varepsilon \le \varepsilon_2 = 100\ \mathrm{eV}$
- and (4) 0.106 for $\varepsilon_2 \le \varepsilon \le \varepsilon_m$

G(i)=0.045+0.850+0.433+0.106[1+6.21G(i)] or G(i)=4.19.

Fig.15

Primary Excitation and Ionization Yields in Liquid Water

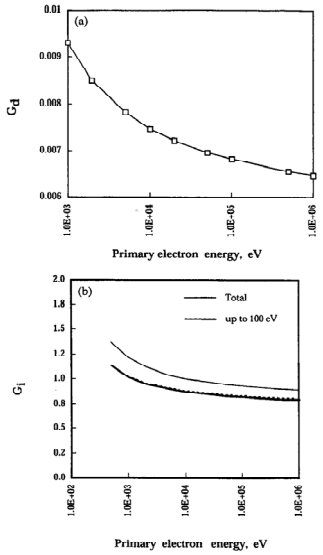

(*a*) Variation with primary energy of the *G* value of dissociation in liquid water induced directly by the primary electron. Notice the very low *G* value and the relatively mild variation with incident energy. (*b*) Variation with primary energy of the *G* value of ionization in liquid water induced directly by the primary electron. The contribution due to all energy losses and those due to $\varepsilon_0 \le \varepsilon \le \varepsilon_2$ are shown separately. Note that these yields are considerably lower than experimental values indicating substantial contribution to ionization by secondary electrons. See text for explanation.

Fig.16

CONCLUSIONS

- Bethe's app. is used with quantum eff. To estimate the first collision yields (ion.+ex.)
- Almost entire diss. Yield in liq. Water may be due to DEA, followed by detachment.
- I.P. of Liq. Water is defined to generate an electron in the conduction band (11.7 eV).
- No evidence foundfor superexcited states in liq. water.
- Cage recombination is unnecessary.

Fig.17

Fig. 14 gives the Born-Bethe procedure for the inelastic scattering cross-section (energy loss) of primary electrons in liquid water, using the so-derived DOSD. The procedure has been slightly modified to incorporate the equipartition between glancing and knock-on collisions. The most important thing in the procedure for calculating the primary yields, indicated in fig.15, is the inclusion of experimental values of ionization and excitation efficiencies, which has hitherto been ignored. The result is shown in fig.16 for the primary excitation and ionization yields in liquid water as a function of primary electron energy. The primary ionization yield can be rationalized with the experimental total ionization yield by a heuristic procedure, based partly on energy balance and partly on an $(energy)^{-2}$ variation of cross-section for the production of secondary electrons. Such a procedure is not available for excitation yield. Also notice that the neutral excitation yields are very small with a G-value (≤ 0.1), so that these states cannot be the source of primary H-atoms, as we have remarked earlier. Fig. 17 states our conclusion about the primary processes in liquid water including excitation, ionization and DEA . The lack of evidence for superexcited states and the cage effect are stressed *only for liquid water*.

3. The quasi-ballistic model of electron mobility in liquid hydrocarbons

In this section we will describe the quasi-ballistic model of electron mobility in liquid hydrocarbons in all its ramifications, viz. the development of basic theory and comparison

with experimental results (fig.18-22), thermodynamic consequence (fig.23-26), field-dependent mobility (fig.27-29), theory of scavenging (fig.30-33) and the relationship between free-ion yield and mobility (fig.34 -37).

Quasi-Ballistic Model of Electron Mobility

Langevin Eq. : $d<v>/dt = -\zeta + eE/m$; $\mu_{qf} = e/m\zeta$ (friction co-eff.)
Integratio n $\rightarrow l(t) = v_d\{1-\zeta^{-1}[1-\exp(-\zeta t)]\}$, with $v_d = \mu_{qf}E$

Prob. density of trapping $\rightarrow \tau_f^{-1}\exp(-t/\tau_f)$; τ_f is mean lifetime in free state.
Distance per trappi ng $<\Delta x> = (eE/m)\tau_f^2/(1+\zeta\tau_f)$.
Cycles of trapping and detrapping per unit time $= 1/(\tau_f + \tau_t)$;
τ_t = life in trapped state.

Effective mobility $\mu_{eff}^{-1} = <\mu>_T^{-1} + <\mu>_F^{-1}$
$<\mu>_T = (e/m)\tau_f^2/(\tau_t + \tau_f)$ (Ballistic) and $<\mu>_F = \mu_Y\tau_f/(\tau_t + \tau_f)$
(Trap - controlled)

Fig.18

Equilibrium Trapping and Detrapping Rates

Trapping rate $k_{ft} = \tau_f^{-1}$; Detrapping rate $k_{tf} = \tau_t^{-1}$

$k_{ft}/k_{tf} = n_t h^3 (2\pi m k_B T)^{-3/2}\exp(\varepsilon_0/k_B T)$)
(Ascarelli and Brown)

(Random Walk Model) : $k_{tf} = (\varepsilon_0/h)\exp(-\varepsilon_0/k_B T)$

$k_{ft} = n_t h^2 \varepsilon_0 (2\pi m k_B T)^{-3/2}$

Fig.19

Effective Electron Mobility

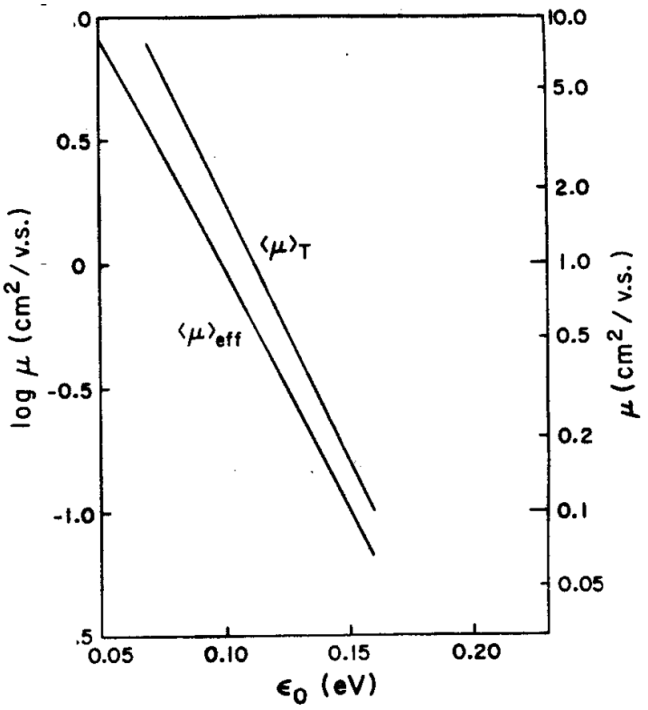

Fig.20

Temperature Dependence of Mobility

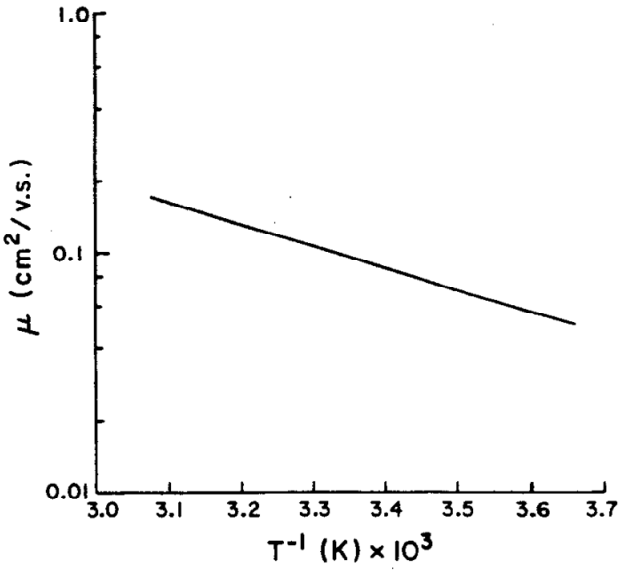

Fig.21

Variation of effective mobility with reciprocal effective temperature. Data for *n*-hexane.

Electron Mobility Parameters in Hydrocarbon Liquids

Table 1
Electron mobility, activation energy, quasi-free mobility and trap density in selected hydrocarbon liquids

Liquid	T (K)	μ [a]	E_a(exp.) [c]	E_a(calc.) [d]	n_t [b]	ϵ_0 [e]
propane	273	1.46	0.155	0.175	0.14	0.137
pentane	295	0.15	0.19	0.224	0.45	0.168
cyclopentane	293	1.1	0.12	0.160	0.78	0.106
n-hexane	295	0.1	0.2	0.170	1.0	0.150
cyclohexane	295	0.45	0.13	0.170	1.2	0.111
ethane	216	0.8	0.1	0.125	0.4	0.088
butane	300	0.4	0.13	0.175	1.1	0.115
benzene	300	0.114	0.32	0.324	0.012	0.284
isooctane	296	4.5	0.05	0.055	0.675	0.044
3-methyl pentane	293	0.2	0.2	0.225	0.27	0.174
isobutene	293	1.44	0.1	0.141	1.0	0.088

[a] In $cm^2 V^{-1} s^{-1}$; experimental data from Refs. [2] and [21]. Theoretical calculation is matched with experimental determination (see text).
[b] In $10^{19} cm^{-3}$. [c] Experimental value, eV.
[d] Recalculated theoretical value, eV, using the input parameters so-determined.
[e] Electron binding energy in trap, eV.

Fig.22

The quasi-ballistic model of electron mobility derives from finite momentum relaxation time in the quasi-free state , following detrapping of the electron. A competition between trapping and momentum relaxation occurs, resulting in the effective mobility given both by the usual trap-controlled mobility and a mobility, due only to random trapping and detrapping, which has been called the ballistic mobility. As shown in fig.18, the effective mobility is a function of quasi-free mobility, lifetimes of the electron in the trapped and quasi-free state and the density of traps. Fig.19 gives the trapping and detrapping rates in terms of the equilibrium ratio of these rates calculated by Ascarelli and Brown and an absolute detrapping rate calculated by Mozumder on the basis of a random walk model. Fig. 20 is a model calculation of the variation of the effective mobility with the binding energy of the electron in the trap, while fig.21 shows an approximate Arrhenius temperature dependence in a typical case. Comparison with experimental results for low- and intermediate-mobility liquids ($\mu_{eff} \sim 0.1 to \sim 5 cm^2 v^{-1} s^{-1}$) , as shown in fig.22, indicates that in most of these liquids the trap density is $\sim 10^{19} cm^{-3}$ and the binding energy in the trap lies in the interval $\varepsilon_0 \sim 0.1 to 0.2 eV$.

Thermodynamic Parameters for Electron Trapping

$$K_{tr} \equiv k_{ft} / k_{tf} = n_t h^3 (2\pi m k_{BT})^{-3/2} \exp(\varepsilon_0 / k_{BT})$$

$$\Delta G_{tr} \equiv -k_{BT} \ln K_{tr}; \text{Standard} T_0 = 298K; n_t^0 = 10^{19} cm^{-3}.$$

$$\Delta G_{tr}^0 = -\varepsilon_0 - 2.3927(T/T_0)[\ln n_t - (3/2)\ln(T/T_0) - 0.1728]$$

$$\Delta G_{tr}^0 = \Delta H_{tr}^0 - T\Delta S_{tr}^0$$

Fig.23

Free-Energy Change in Trapping

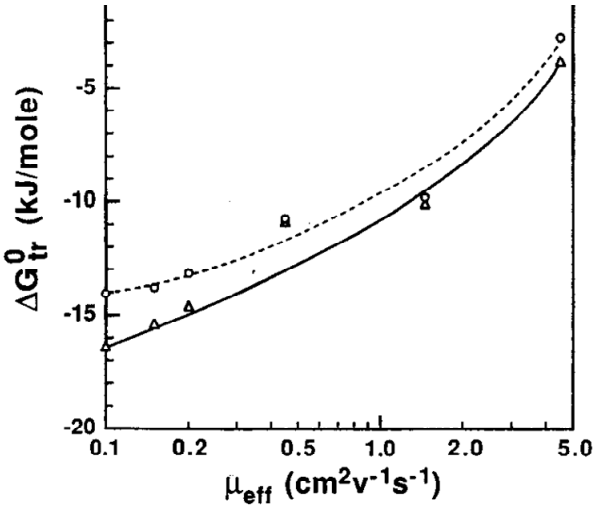

Standard free energy change on electron trapping from the quasi-free state vs effective electron mobility in various liquid hydrocarbons according to the quasi-ballistic (O) and the usual trapping (△) models of mobility.

Fig.24

Free-Energy Change on Solvation

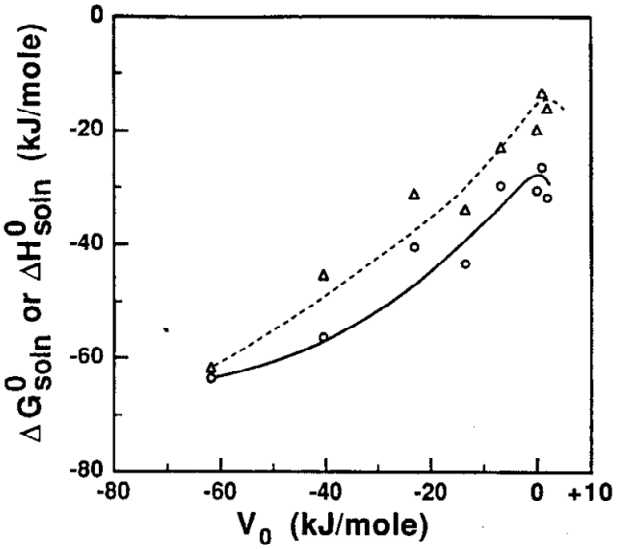

Standard free energy (—, ○) and enthalpy (- - -, △) of electron solvation in hydrocarbon liquids vs V_0, the energy of the lowest conducting state in the liquid. See text for details.

Fig.25

Thermodynamic Conclusions

- Electron solvation in hydrocarbon liquids from vacuum proceeds both by negative enthalpy and positive entropy changes. However, entropy change on trapping from quasi-free state is negative (enthalpy driven process).
- Negative entropy change on trapping may be consistent with Anderson's model of localization.
- In low and intermediate-mobility liquids, the attachment rate in the quasi-free state greatly exceeds the overall rate, while the detachment rates are nearly equal.
- Efficiency of attachment reaction generally falls with electron mobility. Only in liquids of lowest mobility can the diffusion-controlled reaction be seen.

Fig.26

Fig. 23 gives the thermodynamic parameters for trapping directly in terms of the equilibrium ratio of trapping and detrapping rates. Because of the linear variation of free-energy with T in most cases, the enthalpy and the entropy changes for the trapping process are clearly separated. In this context, trapping means a transfer of the electron from the quasi-free to the trapped state. Solvation, on the other hand, means a transfer of the electron from vacuum to the trapped state in the liquid. As discussed by Holroyd, evaluation of the thermodynamic parameters of solvation needs further experimental results and assumptions. We have used the same procedure for liquid hydrocarbons. The results are shown in fig.24 and 25 respectively for trapping and solvation. The conclusions are summarized in fig.26. In short, the solvation process is aided both by negative enthalpy and positive entropy changes. The trapping process, on the other hand, is governed only by a negative enthalpy change, being opposed by a negative entropy change on trapping. The trapped state is more ordered. This has a natural explanation in the Anderson model of localization to be discussed later.

Field –Dependence of Mobility

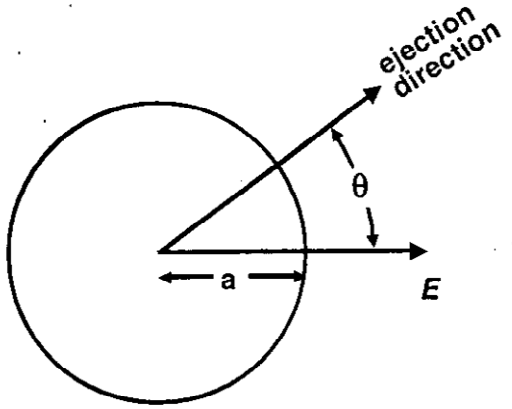

Electron detrapping process in the presence of an external field E. The direction of ejection makes an angle θ relative to the field direction, causing detrapping barrier to change from ε_0 to $\varepsilon_0 + eaE\cos\theta$, where a is the trap radius.

Fig.27

Field-Dependent Mobility: Quasi-Ballistic Model

Low - mobility Liquids : $k_{ft} >> k_{tf}$.

Only k_{tf} effected by the external field E.

$$\varepsilon_0 \rightarrow \varepsilon_0 + eaE\xi; \xi = \cos\theta$$

$$< k_{tf} >_E = k_{tf}(1/2)\int_{-1}^{+1} \exp(-eaE\xi / k_B T)d\xi = k_{tf}\frac{\sinh\eta}{\eta}$$

$$\eta = eaE / k_B T$$

Critical Field for 10% mobility increase

$$E_c = 0.775(k_B T / ea)$$

Fig.28

Critical Field and Trap Radius

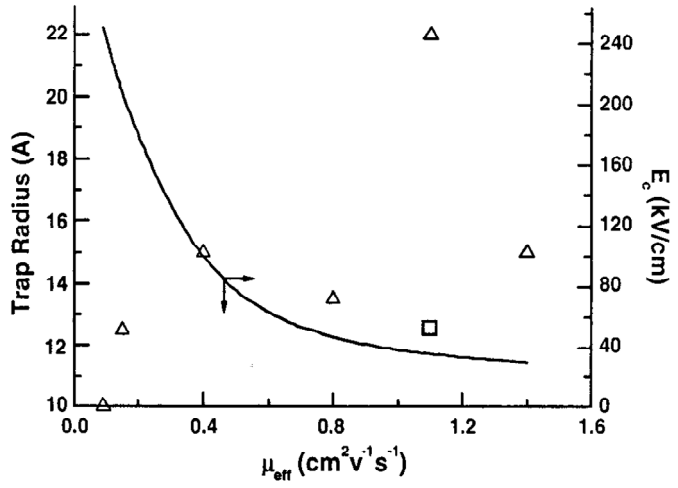

Variation, with zero-field mobility μ_{eff}, of the critical field E_c for nonlinearity in low-mobility hydrocarbon liquids. A clear trend is observed for normal alkanes with a precipitous fall of E_c for μ_{eff} above 0.5 $cm^2\ V^{-1}\ s^{-1}$ (right scale, solid curve). The calculated trap radius, or the extent of the trapped electron wave function (left scale, triangles) do not bear any systematic relationship with either μ_{eff} or E_c.

Fig.29

The field dependence of mobility for low-mobility cases (supralinear) is of special significance to the quasi-ballistic model. As shown in fig.27, the direction of ejection relative to the external field direction, is important as it changes the binding energy in the trap. Fig. 28 gives the effect of this changed binding energy on the effective mobility. As in the hopping model, the quasi-ballistic model also gives a sinh-dependence of the effective mobility on the external field strength. However, the interpretations are quite different. In the hopping model the derived length parameter refers to the hopping distance, while, in the quasi-ballistic model, it refers to the trap size. We can define a critical field at which the measured mobility increases by ~10% from its value at zero field. This critical field is related to the trap radius and both are shown in fig. 29 as functions of the zero field mobility.

Electron Scavenging in Quasi-Ballistic Model

Prob. of finding electron in qf, trapped or scavenged state :

π_f, π_t, π_s with $\pi_f + \pi_t + \pi_s = 1$

$\dot{\pi}_f = -(\lambda_s + k_{ft})\pi_f + k_{tf}\pi_t;\ \dot{\pi}_t = -k_{tf}\pi_t + k_{ft}\pi_f;\ \lambda_s = k_s^f c_s$

With reasonable approximation : $\pi_s(t) = 1 - \exp(-\beta t)$

$\beta = \lambda_s k_{tf}/(k_{ft} + k_{tf})$. Define $k_s^{eff} = \beta / c_s = k_s^f k_{tf}/(k_{tf} + k_{ft})$

$k_s^f = 4\pi D_0 a \eta/(1 + d/2a)$ Fractal result Reaction efficiency is η.

Fig.30

Re-Encounter Probability and Reaction Rate

$$\beta = \kappa/[1-(1-\kappa)P(L)];\ \beta \rightarrow \text{Total Re-encounter Probability}$$

$$P(L) \doteq 1-\exp(-r_c/L)[1+(d/L)/(1+d/r_c)];\ L \propto l$$

$$k_r/k_D = \beta/(1+d/r_c)$$

Fig.31

Reaction Efficiency vs. Electron Mobility

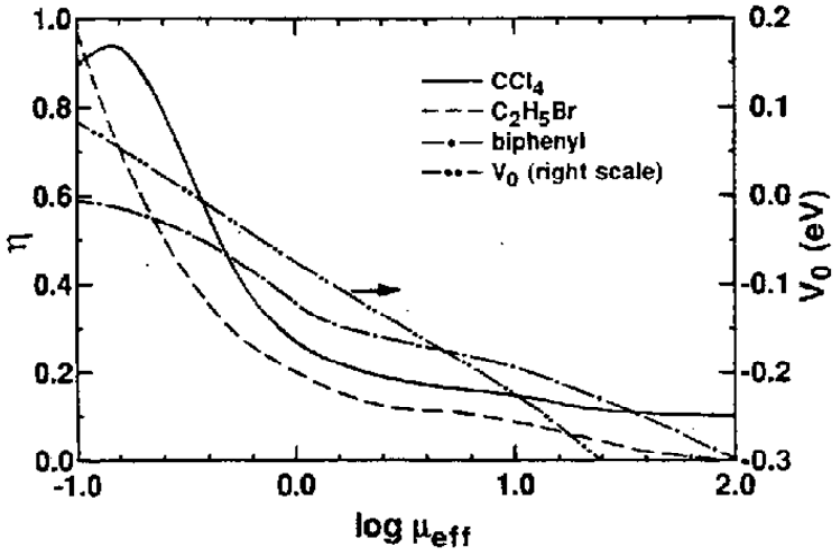

Reaction efficiency η vs log μ_{eff} ($cm^2\ V^{-1}\ s^{-1}$) for CCl_4, C_2H_5Br, and biphenyl in various hydrocarbon liquids (see text for explanation).

Fig.32

Electron Attachment Rate in Quasi-Free State

Electron Attachment Reaction in Liquid Hydrocarbons: Reaction Rate and Efficiency in the Quasi-Free State[a]

solvent	solute	T (K)	k_1	k_1^f	k_{diff}	η	remark
n-hexane	styrene	329.4	1.9×10^{12}	3.04×10^{14}	4.68×10^{14}	0.650	*
	α-methylstyrene	329.6	1.4×10^{12}	2.26×10^{14}	4.68×10^{14}	0.483	†
	p-$C_6H_4F_2$	296	9.1×10^{11}	3.14×10^{14}	4.38×10^{14}	0.717	*
cyclohexane	*p*-$C_6H_4F_2$	298	2.5×10^{12}	2.21×10^{14}	4.40×10^{14}	0.502	†
isooctane	naphthalene	361.3	9.0×10^{12}	2.6×10^{13}	4.95×10^{14}	0.0525	‡
	styrene	321.0	1.2×10^{13}	4.4×10^{13}	4.61×10^{14}	0.0954	‡
	α-methylstyrene	299.1	1.5×10^{13}	6.3×10^{13}	4.42×10^{14}	0.1425	‡
	CO_2	306.0	6.94×10^{12}	2.84×10^{13}	4.47×10^{14}	0.0635	‡
neopentane	CO_2	297	5.5×10^{11}	7.86×10^{11} [b]	4.38×10^{14}	1.8×10^{-3}	‡
tetramethylsilane[c]	triphenylene	322.9		2.0×10^{13}	4.63×10^{14}	0.0432	‡
	phenanthrene	307.7		1.4×10^{13}	4.50×10^{14}	0.0311	‡
	naphthalene	273.1		1.0×10^{13}	4.17×10^{14}	0.0240	‡
	styrene	237.7		1.4×10^{13}	3.82×10^{14}	0.0366	‡
	α-methylstyrene	219.5		1.5×10^{13}	3.64×10^{14}	0.0412	‡

[a] All specific rates in M^{-1} s^{-1}. [b] Taken as $k_1^f = k_1 \mu_q / \mu_{eff}$ with $\mu_{eff} = 70$ cm^2 V^{-1} s^{-1}. [c] In tetramethylsilane $k_1 = k_1^f$ in the absence of trapping.

Fig.33

Basic equations for scavenging are developed in fig. 30. These show that, using an approximation which is almost always valid, the effective scavenging rate can be written as $k_{eff} = k_s^f k_{tf} / (k_{tf} + k_{ft})$, where k_s^f is the scavenging rate in the quasi-free state and the rates of trapping and detrapping are as indicated respectively. This expression has an intuitive meaning that the electron is actually scavenged in the quasi-free state and the time available for it is in proportion to the time spent in that state. However, the rate coefficient for scavenging in the quasi-free state requires a special treatment because of the long electron mean free path in that state. Fig. 31 develops this idea in terms of a re-encounter model band a specific probability of reaction at the encounter radius. The so-derived reaction efficiency generally decreases with the effective mobility as shown in Fig.32, by comparison with experimental results. Fig. 33 gives the electron attachment rates in attachment-detachment reactions for various solutes in different hydrocarbon liquids. In very low mobility liquids diffusion-controlled rate may be seen, while in the relatively high mobility liquids clearly the reaction is activation-controlled. For intermediate mobility liquids the reaction is often partially diffusion-controlled.

Empirical Correlation: Free-Ion Yield and Mobility

Empirical Correlation [Jay-Gerin et al.] Can.J.Chem. 71(1993)287.

$$G_{fi} \approx 0.1 \text{ for } \mu < 0.1 cm^2 v^{-1} s^{-1}$$
$$G_{fi} \propto \mu^{0.31} \text{ for } \mu \geq 0.1 \text{cm}^2 v^{-1} s^{-1}$$

Fig.34

Free-Ion Yield and Mobility

Hypothesis : Epithermal (~ 0.2 eV) momentum relaxation requires One effective energy loss (loss - gain) collision

n_{el} (epi) = number of elastic collisions =

$$(k^{-1})\left[\frac{1 - \hbar\omega / E_{epi} + \exp(-\hbar\omega / k_B T)}{1 - \hbar\omega / E_{epi} - \exp(-\hbar\omega / k_B T)}\right]$$

τ_{epi} (epitherma l mom. relax. time) =

$$n_{el} L / v_{epi} \; ; v_{epi} \approx 2.7 x 10^7 \, cm / s.$$

$\mu_{epi} = (e/m)\tau_{epi} \; ; \mu_{qf} = \mu_{epi} (v_{epi} / v_{th}) =$

$2.31 (e/m)\tau_{epi}$ (Lorentz Model)

The free - ion yield is related to theeffect ive mobility by mfp L via trapping and detrapping rates.

Fig.35

Thermalization Distance by Elastic and Inelastic Collisions

Overall Energy Loss $= (E_0 - 3k_BT/2) - (e^2/\varepsilon R_0)(1 - R_0/r_{th})$

$n_g / n_l = (1 - \hbar\omega / E)^{-1} \exp(-\hbar\omega / k_BT)$

$$n_{in} = (n_l + n_g) = [\frac{1 - \hbar\omega/E + \exp(-\hbar\omega/k_BT)}{1 - \hbar\omega/E - \exp(-\hbar\omega/k_BT)}](\hbar\omega)^{-1}[OEL]$$

$n_{el} = n_{in}/k$. On random walk model $r_{th}^2 = n_{el}L^2$; $L \rightarrow$ elastic mfp.

$r_{th}^2 = (L^2/k)n_{in}$. Implicit Equation for r_{th}.

Fig.36

Free-Ion Yield and Scattering Mean Free Paths

Free-ion Yield, Scattering Mean Free Path and Probability of Inelastic Collision for Low-mobility Liquids

liquid	G_{fi}[a]	b (Å)[b]	ϵ[c]	L (Å)[d]	k[e]
toluene	0.09	43	2.38	1.15	0.10
m-xylene	0.08	41	2.37	1.04	0.09
n-octane	0.13	58	1.95	2.91	0.25
trans-but-ene	0.08	53	1.84	2.55	0.22
1,2,3,4-tetramethylbenzene	0.11	42	2.54	1.06	0.09

[a] Free-ion yield per 100 eV of deposited energy at ~300 K. [b] Thermalization distance parameter from ref 5. [c] Dielectric constant from ref 5. [d] Elastic mean free path from this work. [e] Ratio of inelastic to elastic cross sections from this work.

Free-ion Yield and Mobility Data for Intermediate and High Mobility Liquids[a]

liquid	G_{fi}[b]	μ_{eff}[c]	ϵ[d]	ϵ_{ac}[e]	b (Å)[f]
3-methylpentane	0.18	0.2	1.90	0.20	67
cyclohexane	0.20	0.45	2.02	0.13	59
isooctane	0.35	4.5	1.94	0.05	110
2,3-dimethylbut-2-ene	0.44	6.0	1.98	0.055[g]	102
isobutane	0.51	7.3	1.74	0.055[g]	116
neohexane	0.58	12.0	1.87	0.06	120
tetramethyltin	0.63	78.0	2.25	0.014[h]	115
tetramethylgermanium	0.66	90.0	2.01	0.014[h]	143

[a] Experimental data on free-ion yield and mobility, to which our calculated values are nominally equated, are literature based. Since experimental determinations have inherent uncertainties and variations from one laboratory to another, there are no unique, precise values. Those reported here are taken from literature as best-judged. [b] Free-ion yield per 100 eV at ~300 K. [c] Effective mobility at ~300 K (cm^2 v^{-1} s^{-1}). [d] Dielectric constant. [e] Activation energy of mobility (eV). [f] Thermalization distance parameter (ref 5). [g] Assumed. [h] Assumed to be the same as in neopentane.

Fig.37

The rest of this section will be devoted to the relationship between free-ion yield and mobility. In the Onsager theory, there is no direct relation between these two quantities. However, experimentally a clear empirical dependence exists, as shown in fig.34. For very low-mobility liquids, the free-ion yield is independent of the mobility, whereas in other liquids, it increases with the mobility. In terms of the quasi-ballistic model of electron mobility, an explanation has been found. It is that the elastic and inelastic collision cross-sections of the epithermal electron govern both these processes. The elastic collisions determine the momentum relaxation time which gives the epithermal mobility and eventually the quasi-free and effective mobilities through the Lorentz equation and the quasi-ballistic model respectively. At the same time, the elastic and inelastic cross-sections determine the thermalization distance giving the free-ion yield. Thus these two quantities become indirectly correlated.Fig.35 and 36 develop these ideas quantitatively and respectively for mobility and free-ion yield. In very low-mobility liquids, the mobility is determined mainly by the ballistic process, thus the free-ion yield becomes independent of it. Fig.37 gives the scattering mean free paths and the probability of an inelastic collision per scattering, by comparison with experimental results. In low-mobility liquids, the probability of an inelastic collision (energy loss or gain) per scattering event is around ~1/3 to ~1/7. This factor increases progressively with the effective mobility and at the highest mobility the situation resembles that of a liquefied rare gas. The elastic mean free paths are comparable to molecular dimensions in low-mobility liquids, while for higher mobility liquids, it can approach tens of A.

4. Electron localization in hydrocarbon liquids: The Anderson model

In this section will be described electron localization in hydrocarbon liquids by the Anderson model. This was the topic of an invited talk given by A.Mozumder at the ASR 2007 Symposium held in Tokai-Mura during November 6-9, 2007. In this sense this was the highlight of his visit to Japan this year.

First, we need to make a distinction between localization and trapping, the latter requiring medium reorganization. Secondly, many hydrocarbon molecules including n-alkanes lack electron affinity. The corresponding liquids are not known to harbor voids or bubbles, such as found in polar liquids, or in liquid helium. Anderson model does not require any special property of the molecule for localization; what it does require is sufficiently large randomness of site energy so that it can overcome site to site transport by the negotiating potential. It must be remembered that Anderson's model is for localization by static disorder. It must be supplemented by a trapping theory to compare with experimental mobility. Further, one also needs to incorporate a physical basis for the

diagonal disorder, that is, the random fluctuation in site energy. Otherwise, it simply becomes a model study.

Electron Localization

Results from Anderson Theory

G.L.Hug and A.Mozumder
Radiation Laboratory
University of Notre Dame
Notre Dame, In 46556, U.S.A.

Fig.38

INTRODUCTION

- Electron Localization and Connectivity
- The Anderson Model
- Diagonal Disorder
- Scaling Theory
- Results and Summary

Fig.39

Connectivity and Liquid Structure

$$H = \sum_n \varepsilon_n a_n^+ a_n + V \sum_{n,m} a_n^+ a_m$$

$$(W/2V)_c = fK \ln(W/2V)_c \; ; K = Z - 1$$

(W/2V)c

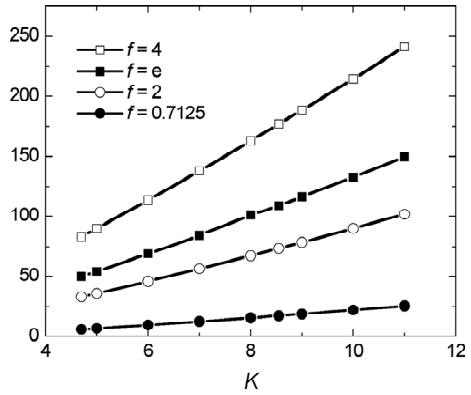

Fig.40

Figs. 38 and 39 give the title, co-author and affiliation with an introduction. Fig. 40 displays the simplest form of the Anderson Hamiltonian in the second quantized form with random site energy ε_n and a deterministic mediating potential V for nearest neighbor transport. The details of the quantum mechanical calculation varies from author to author, but there are general agreements on certain points. First, the actual distribution of the site energy is much less important than the width W of that distribution. Secondly, there is a critical value of W/2V above which no state of the electron may be delocalized and below which both localized and delocalized states my co-exist, however separated sharply an energy, called the mobility edge. The critical value of $(W/2V)_c$ satisfies an equation involving the lattice connectivity K as shown in the displayed equation. While K may be taken to be Z-1, where Z is number of nearest neighbors, the additional parameter in the equation ,f, does depend on the nature of the medium and the actual distribution of site energy. Different authors have used different values of f from 4.0 to 2.0. We have compared the numerical results of Chang et al. with that of Shante and Kirkpatrick for percolation in a cubic lattice and found f to be 0.7125. We have used this value successfully in alkane liquids.

Mobility Edge Trajectory :

Results From Scaling Theory

Wave Function Envelope ~ $\exp(-r/\xi)$

$$\xi(E) \sim [E_c(\sigma\sigma - E]^{-\nu} (E \le E_c).$$

$$\xi(\sigma) \sim [\sigma - \sigma_c(E)]^{-\nu} (\sigma \ge \sigma_c(E)).$$

Fig.41

Mobility Edge Trajectory

Chang et al. (1990)

$$\sigma_c(E) = \sigma_c - AE^2$$

$$\sigma_c(E)/\sigma_c = 1 - \exp[-(E/E_1)^2]$$

Fig.42

For a given disorder $(\sigma \equiv W/2V)$, there is a critical energy E_c below which all states are localized. The envelope of the wave functions satisfies an index equation $\xi(E) \sim [E_c(\sigma) - E]^{-\nu} (E \le E_c)$, which is called the mobility edge trajectory. There is a similar equation when the disorder is approached from above at a given energy, as shown in fig.41. It is a fundamental result of the scaling theory that the indices for the divergence of the wave function is the same when expressed either in terms of energy, or in terms of the disorder. Following Chang et al. we have used $\nu = 1$, consistently and without any difficulty. Further, Chang et al. have invoked a symmetry argument to give the dependence of σ_c on energy. In our case, we have modified their expression to

$\sigma_c(E)/\sigma_c = 1-\exp[-(E/E_1)^2]$, where E_1 is a certain unspecified energy, later to be identified with V. This is displayed in fig. 42. This form satisfies the symmetry argument and also the asymptotic values.

LIQUID STRUCTURE

X-ray Normalized Scattered Intensity I(k)

$$g(r) = \rho + (1/2\pi^2 r)\int_0^\infty k[I(k)-1]\sin krdk$$

$$Z = \int_{r_{\min}}^{r_{\max}} 4\pi r^2 g(r)dr$$

Fig.43

Radial Distribution Function for Ethane

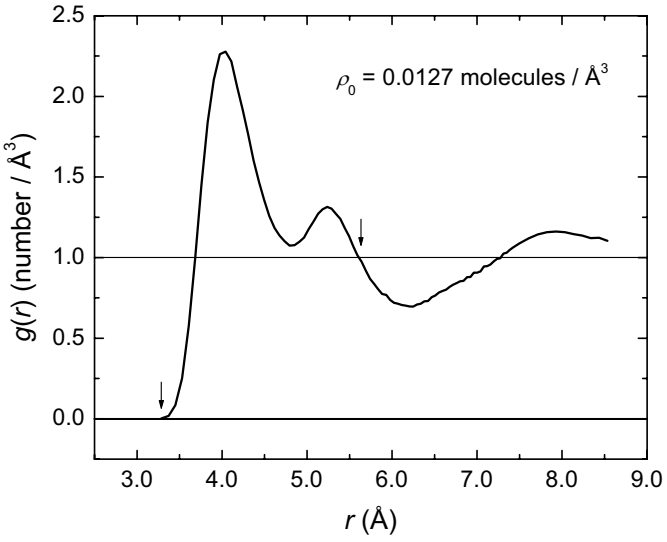

Fig.44

Radial Distribution Function For Propane

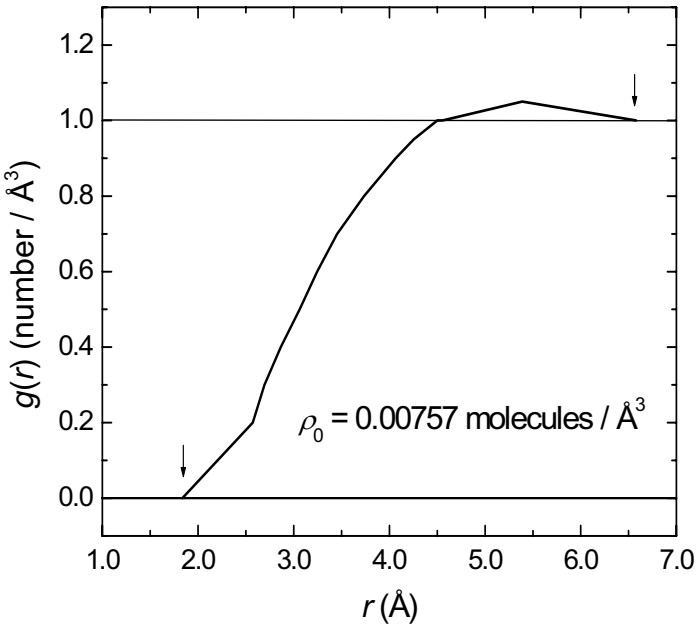

Fig.45

Radial Distribution Function For Butane

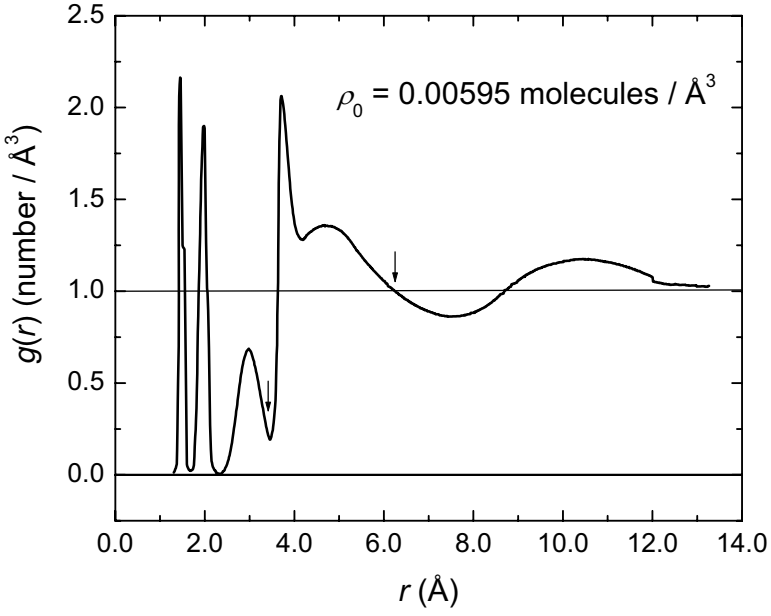

Fig.46

Radial Distribution Function For Neopentane

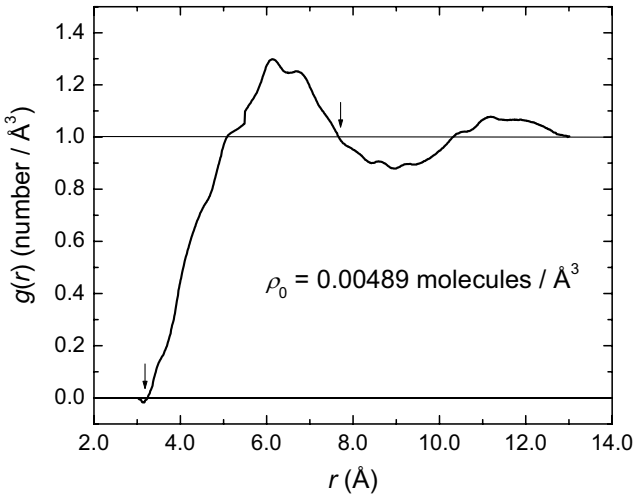

Fig.47

To determine Z, the number of nearest neighbors to a molecule in the liquid and from there to compute K, the connectivity, we employ the radial distribution function (RDF) for that liquid as deduced from small angle X-ray (and sometimes neutron) diffraction. The relation between RDF and the scattered intensity is given in fig.43. Experimental curves for the so-determined RDF are shown in figs.44 through 47 for ethane, propane, butane and neopentane at the specified temperatures. The vertical arrows mark the lower and upper limits of integration to compute Z.

Disorder From Polarizability Anisotropy

$$W = Z[e^2 / 2(r_1 / 2)^4]\left|\alpha_1 - \alpha_2\right|$$

$$\left|V_0\right| = V\sqrt{-\ln(1-\sigma/\sigma_c)} = V\sqrt{-\ln(1-W/2V\sigma_c)}$$

$$\xi_{\max} / \xi_{\min} = [\frac{V_0 - E_{\max}}{V_0 - E_{\min}}]^{-\nu}$$

Fig.48

Diagonal Disorder in n-Alkane Liquids

Liquid	$\bar{\alpha}(A^3)$	$\lvert\alpha_1-\alpha_2\rvert(A^3)$	W(eV)[c]	V_0(eV)[d]	V(eV)[e]
Methane[b]	2.6	0	~0	-0.3	
Ethane	4.47	1.51	1.20	0.2	0.74
Propane	6.29	1.92	1.38	-0.1	0.18
n-butane	8.12	2.18	1.05	0.12	0.1
n-pentane	9.95	3.13	3.46	0.00	
n-hexane	11.78	4.03	4.46	0.02	
n-heptane	13.61	4.57			
n-octane	15.44	5.18			
n-decane	19.10	6.01			
n-dodecane	22.74	8.22			

Fig.49

Characteristics of Localized States in Liquid Hydrocarbons

Liquid	σ	σ_c	% of delocalized states	$\Delta E^b_{act}(eV)$	$\xi^c_{\max}(A)$
Methane[d]	0	25.34	100		
Ethane	0.81	17.37	97.6	0.1	55
Propane	3.83	12.95	83.9	0.16	96
n-butane	5.25	7.32	53.2	0.13	81
n-pentane	17.3[e]	6.86	0	0.19	95
n-hexane			0	0.2	100

Fig.50

In our model, the diagonal disorder, or the random fluctuation of site energy originates from the anisotropic polarizability interaction of the electron with the molecule. This depends on the location of the electron relative to that of the molecule. The width of

fluctuation is then given by the difference between the maximum and minimum polarizabilities, which can be determined directly from depolarized Rayleigh scattering. Considering V_0 as the minimum energy of a delocalized electron an implicit equation for V has been derived in terms of $V_0 and \sigma_c$. This is shown in fig. 48. Fig. 49 gives the mean polarizabilities $(\overline{\alpha})$ and the difference between maximum and minimum polarzabilities $|\alpha_1 - \alpha_2|$ of molecules in the alkane series. We see that the mean polarizability increases with the carbon number (size effect) and the anisotropy also increases, i.e., the molecules become progressively 'cigar-like'. From the known values of V_0, it is then easy to calculate V, the interaction energy within the context of the Anderson model. This is important, because no independent calculation is at present available for that energy. The so-determined values of V are shown in fig.49 for ethane, propane and butane. Fig. 50 gives the characteristics of electron states in alkane liquids in terms of the percentage of initially delocalized states. At present, it is the nature of the states, irrespective of their occupation. Our calculations indicate 100% delocalization in liquid methane (all components of polarizability are equal) and 0% for n-pentane, n-hexane and so on. It is surprising that we calculate initial delocalization in ethane and propane as 98% and 84% respectively. Electron mobility in these liquids are known to be low. However, as we have alluded to before, the initial delocalization can be drastically changed due to trapping and by thermal fluctuation.

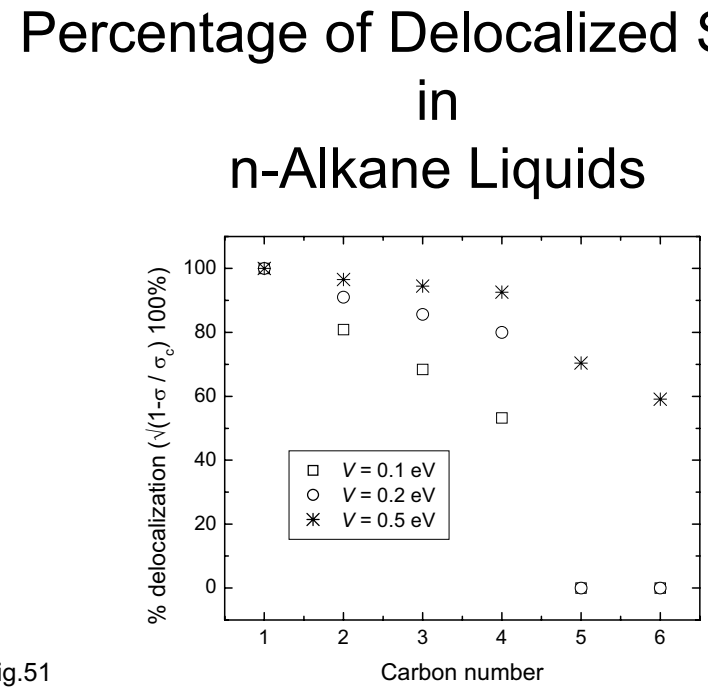

Fig.51

CONCLUSIONS

- We have applied the Anderson model for the initial localization of low-energy electrons in liquid hydrocarbons. We find that both the liquid structure (g(r)) and molecular polarizability (symmetry) are important for electron localization.
- The electron energy fluctuation (diagonal disorder) is taken to originate from electron molecule anisotropic polarizability interaction.
- According to our calculations, the initial states in liquids of highly symmetrical molecules (methane,NP,TMS etc.) are fully delocalized, those in ethane and propane are largely delocalized. In liquid butane, the initial states are partially delocalized, while in pentane onwards, these are fully localized.
- Trapping and contact with heat bath will change the situation somewhat. Trapping cross-sections are indicated in the range of ~900A2, however more work is necessary for describing trapping from the doorway states.

Fig.52

Fig. 51 shows a model study of percentage of delocalized states in liquid alkanes vs. the carbon number. In this study we have not insisted on the self-consistency of the interaction energy V , but left it as a floating parameter within a range of possible values. Fig. 52 summarizes our conclusions on the Anderson localization of electrons in alkane liquids. One point is most important, that is both the liquid state connectivity and the anisotropy of molecular polarizability are important for *initial* localization. What remains to be done to make the theory complete is to study the effect of thermal fluctuation and that of trapping. Work is in progress.

5. Free-ion yield in liquefied rare gases: A new theoretical model

MeV Electron Track in LAR

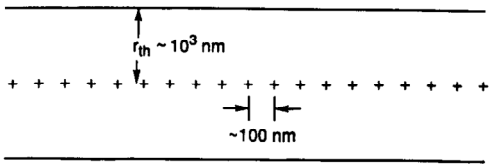

Fig. 1. Model of a low-LET track in liquid argon. The positive ions (Ar_2^+) are immobile on the axis separated by $\sim 10^2$ nm. Electron thermalization length is $\sim 10^3$ nm; thus the geometry approximates a cylindrical symmetry rather than a collection of isolated ionizations, each with spherical symmetry. This is true even at the minimum LET.

Fig.53

Free-Ion Yield in LRG at Low-LET

$$N_R = \kappa \sum n_+^s L_s ; n_+^{s+1} = (1-\kappa) n_+^s ; L_{s+1} = L_s - \mu E \tau_s$$

$$r_1^{s+1} / r_2 = (r_1^s / r_2)^{1/(1-\kappa)} ; r \rightarrow CTP; r_2 \rightarrow inner\ radius.$$

$$\tau_s = \varepsilon (r_1^s)^2 / 2\mu n_+^s e; \sum_{s=1}^{m} \tau_s \le L_0 / \mu E; V_d = \mu E$$

$$N_R = n_+^0 L_0 [1-(1-\kappa)^{m+1}] - V_d n_+^0$$
$$\text{x}[\sum \tau_s (1-\kappa)^{m+1} - (1-\kappa)^{m+1} \sum \tau_s$$

$$P_R = N_R / n_+^0 L_0 ; P_{esc} = 1 - P_R ; P_{fi} = (1 + k_r c_0 t_c)^{-1}$$

Fig.54

Free-Ion Yield in LAr; Theory and Experiment

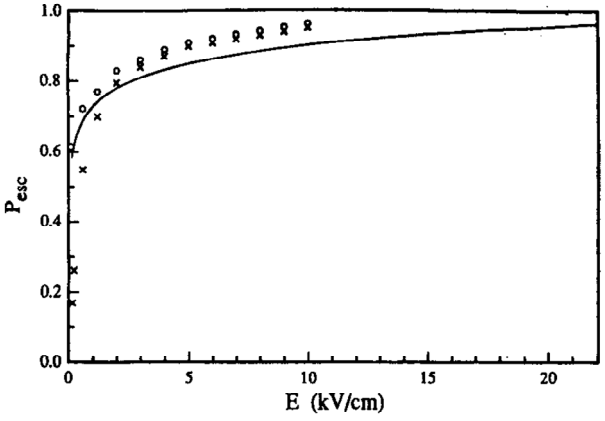

Variation of escape probability with external field in liquid argon at low-LET (1 MeV electron). Full curve, absolute calculated value with $\kappa = 0.01$, $r_0 = r_{th} = 1568$ nm and other parameters as described in text. Experimental points [13] and calculated values normalized to 22 kV/cm are denoted by (×) and (○) respectively.

Fig.55

LAr : Dependence of Escape Probability on Initial Separation

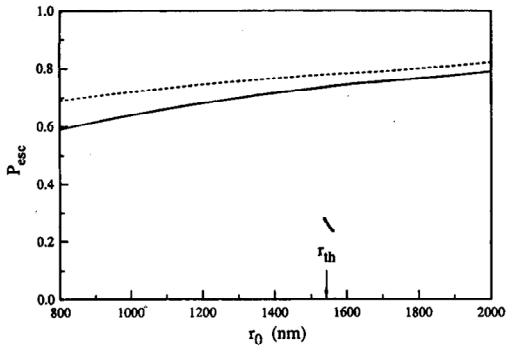

Effect of initial separation (r_0) on the escape probability P_{esc} in LAr at an external field $E = 1200$ V cm^{-1}. Solid line, absolute values of P_{esc}; dashed line, normalized to P_{esc} at 22 kV cm^{-1}. $\kappa = 0.01$; see text for values of other parameters.

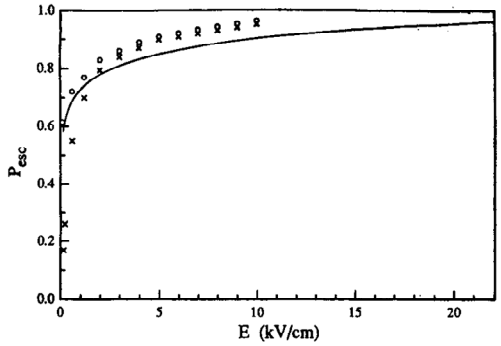

Variation of escape probability with external field in liquid argon at low-LET (1 MeV electron). Full curve, absolute calculated value with $\kappa = 0.01$, $r_0 = r_{th} = 1568$ nm and other parameters as described in text. Experimental points [13] and calculated values normalized to 22 kV/cm are denoted by (×) and (○) respectively.

Fig.56

Free-Ion Yield in LKr: Theory and Experiment

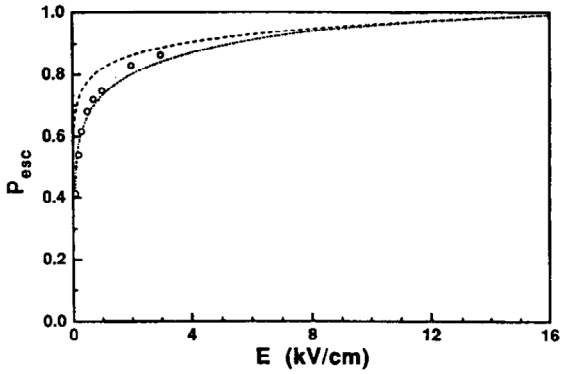

Comparison of calculated and experimental probability P_{esc} of escaping electron–ion recombination in LKr, for a low-LET incident particle, as a function of external field. (– ·) experimental data of Aprile et al. [7] and of Kubota et al. [19]; (–) present calculation with $r_0 = 4000$ nm and $\kappa = 0.1$. (○) indicate a correction due to homogeneous recombination at low fields (see text for details).

Fig.57

CONCLUSIONS

- Onsager's theory is not applicable to LRG at any LET, because ionizations are not isolated.
- Jaffe's theory is also not applicable because it ignores e-ion interaction.
- Re-encounter model captures the basic physics in consistence with track structure, electron mobility and recombination rate.
- For LAr, electron thermalization length~1500 nm and an encounter recombination probability~0.01 are found to describe the experiments.

Fig.58

Fig. 53 shows an MeV electron track in liquid argon (LAr). It is clear that, even for this minimum ionizing radiation, electron thermalization distance is an order of magnitude greater than the mean positive ion separation on the track, computed from the W-value and the LET. Thus, the Onsager equation for the escape probability is not applicable, because the ionizations are not isolated. The cylindrical track models of Jaffe and of Krammers are also not applicable , because of the neglect of the coulombic field in one case and equating the diffusion coefficients of the electron and of the positive ion in the other. It is well-known that in liquefied rare gases the positive ions immediately dimerize, giving very low mobility. Realizing that there is at present no suitable track model for electron-ion recombination in liquefied rare gases (LRG), we developed a re-encounter model. In this model, currently limited to parallel external fields , the electrons are drawn to the track axis by the cylindrical field due to the line of positive charges while being separated axially at the track ends. After an unsuccessful recombination, the electrons, by virtue of their energy, go out to the ever increasing classical turning point and then return for the next trip. This process can go on only for a finite number of return trips until the external field completely separates the charge distributions. At each encounter on the track axis, the electrons have a small probability of recombination which can be computed from the known rate of volume recombination with the aid of a re-encounter theory. The relevant equations are developed in fig.54 which are slf-explanatory. Fig. 55 compares the results of our calculation with experiment. Although the agreement is satisfactory, this by itself cannot be taken as a

validity of the implied theoretical concepts. Similar agreement has been obtained for the Jaffe, or Krammers model as well, with no internal consistency and having completely different theoretical ideas. Also, in our case, the effect of the perpendicular field is unknown and very difficult to analyze. In any case, we have examined the dependence of the escape probability in LAr with the initial or thermalization distance, using the re-encounter model. We find, as shown in fig.56, that the escape probability is relatively insensitive to the initial separation in its important range. If this holds, it may not be necessary to compute the thermalization distance accurately, in contrast with the Onsager model. In fig. 57, we show the results of a similar calculation for liquid krypton. The agreement with experiment, when adjusted for the best recombination coefficient, is equally satisfactory as in the case of LAr, but again it should not be over-emphasized. Our tentative conclusions are summarized in fig.58. These are : (1) neither the Onsager theory, nor the theories of Jafee and Krammers is applicable to LRG. (2)Re-encounter model captures the essential physics of the problem, although the treatment of the perpendicular field is still a problem. (3) In liquid krypton, we find the thermalization length ~ 1500 nm and the recombination probability at an encounter ~0.01.

6. Summary

The electron is the single most important entity in the interaction of charged particles with matter. It appears as the incident radiation both as a primary in some cases, and always as a secondary in ionization processes (delta-rays). In most cases it is also a reactant. Importance of condensed matter is underscored for application to biology (liquid water), industry (liquid hydrocarbons) and high-energy physics experiments (liquefied rare gases). Therefore, various aspects of the electron in condensed media, e.g., its yield, mobility and chemical reaction, are central to irradiation effect.

This is a blank page.

国際単位系（SI）

表１．SI 基本単位

基本量	SI 基本単位	
	名称	記号
長さ	メートル	m
質量	キログラム	kg
時間	秒	s
電流	アンペア	A
熱力学温度	ケルビン	K
物質量	モル	mol
光度	カンデラ	cd

表２．基本単位を用いて表されるSI組立単位の例

組立量	SI 基本単位	
	名称	記号
面積	平方メートル	m^2
体積	立法メートル	m^3
速さ，速度	メートル毎秒	m/s
加速度	メートル毎秒毎秒	m/s^2
波数	毎メートル	m^{-1}
密度（質量密度）	キログラム毎立法メートル	kg/m^3
質量体積（比体積）	立法メートル毎キログラム	m^3/kg
電流密度	アンペア毎平方メートル	A/m^2
磁界の強さ	アンペア毎メートル	A/m
（物質量の）濃度	モル毎立方メートル	mol/m^3
輝度	カンデラ毎平方メートル	cd/m^2
屈折率	（数の） 1	1

表５．SI 接頭語

乗数	接頭語	記号	乗数	接頭語	記号
10^{24}	ヨタ	Y	10^{-1}	デシ	d
10^{21}	ゼタ	Z	10^{-2}	センチ	c
10^{18}	エクサ	E	10^{-3}	ミリ	m
10^{15}	ペタ	P	10^{-6}	マイクロ	μ
10^{12}	テラ	T	10^{-9}	ナノ	n
10^{9}	ギガ	G	10^{-12}	ピコ	p
10^{6}	メガ	M	10^{-15}	フェムト	f
10^{3}	キロ	k	10^{-18}	アト	a
10^{2}	ヘクト	h	10^{-21}	ゼプト	z
10^{1}	デカ	da	10^{-24}	ヨクト	y

表３．固有の名称とその独自の記号で表されるSI組立単位

組立量	SI 組立単位			
	名称	記号	他のSI単位による表し方	SI基本単位による表し方
平面角	ラジアン(a)	rad		$m \cdot m^{-1}=1$(b)
立体角	ステラジアン(a)	sr(c)		$m^2 \cdot m^{-2}=1$(b)
周波数	ヘルツ	Hz		s^{-1}
力	ニュートン	N		$m \cdot kg \cdot s^{-2}$
圧力，応力	パスカル	Pa	N/m^2	$m^{-1} \cdot kg \cdot s^{-2}$
エネルギー，仕事，熱量	ジュール	J	N・m	$m^2 \cdot kg \cdot s^{-2}$
工率，放射束	ワット	W	J/s	$m^2 \cdot kg \cdot s^{-3}$
電荷，電気量	クーロン	C		s・A
電位差（電圧），起電力	ボルト	V	W/A	$m^2 \cdot kg \cdot s^{-3} \cdot A^{-1}$
静電容量	ファラド	F	C/V	$m^{-2} \cdot kg^{-1} \cdot s^4 \cdot A^2$
電気抵抗	オーム	Ω	V/A	$m^2 \cdot kg \cdot s^{-3} \cdot A^{-2}$
コンダクタンス	ジーメンス	S	A/V	$m^{-2} \cdot kg^{-1} \cdot s^3 \cdot A^2$
磁束	ウエーバ	Wb	V・s	$m^2 \cdot kg \cdot s^{-2} \cdot A^{-1}$
磁束密度	テスラ	T	Wb/m^2	$kg \cdot s^{-2} \cdot A^{-1}$
インダクタンス	ヘンリー	H	Wb/A	$m^2 \cdot kg \cdot s^{-2} \cdot A^{-2}$
セルシウス温度	セルシウス度(d)	℃		K
光束	ルーメン	lm	cd・sr(c)	$m^2 \cdot m^{-2} \cdot cd=cd$
照度	ルクス	lx	lm/m^2	$m^2 \cdot m^{-4} \cdot cd=m^{-2} \cdot cd$
（放射性核種の）放射能	ベクレル	Bq		s^{-1}
吸収線量，質量エネルギー分与，カーマ	グレイ	Gy	J/kg	$m^2 \cdot s^{-2}$
線量当量，周辺線量当量，方向性線量当量，個人線量当量，組織線量当	シーベルト	Sv	J/kg	$m^2 \cdot s^{-2}$

(a)ラジアン及びステラジアンの使用は、同じ次元であっても異なった性質をもった量を区別するときの組立単位の表し方として利点がある。組立単位を形作るときのいくつかの用例は表４に示されている。
(b)実際には、使用する時には記号rad及びsrが用いられるが、習慣として組立単位としての記号“１”は明示されない。
(c)測光学では、ステラジアンの名称と記号srを単位の表し方の中にそのまま維持している。
(d)この単位は、例としてミリセルシウス度m℃のようにSI接頭語を伴って用いても良い。

表４．単位の中に固有の名称とその独自の記号を含むSI組立単位の例

組立量	SI 組立単位		
	名称	記号	SI 基本単位による表し方
粘度	パスカル秒	Pa・s	$m^{-1} \cdot kg \cdot s^{-1}$
力のモーメント	ニュートンメートル	N・m	$m^2 \cdot kg \cdot s^{-2}$
表面張力	ニュートン毎メートル	N/m	$kg \cdot s^{-2}$
角速度	ラジアン毎秒	rad/s	$m \cdot m^{-1} \cdot s^{-1}=s^{-1}$
角加速度	ラジアン毎平方秒	rad/s^2	$m \cdot m^{-1} \cdot s^{-2}=s^{-2}$
熱流密度，放射照度	ワット毎平方メートル	W/m^2	$kg \cdot s^{-3}$
熱容量，エントロピー	ジュール毎ケルビン	J/K	$m^2 \cdot kg \cdot s^{-2} \cdot K^{-1}$
質量熱容量（比熱容量），質量エントロピー	ジュール毎キログラム毎ケルビン	J/(kg・K)	$m^2 \cdot s^{-2} \cdot K^{-1}$
質量エネルギー（比エネルギー）	ジュール毎キログラム	J/kg	$m^2 \cdot s^{-2} \cdot K^{-1}$
熱伝導率	ワット毎メートル毎ケルビン	W/(m・K)	$m \cdot kg \cdot s^{-3} \cdot K^{-1}$
体積エネルギー	ジュール毎立方メートル	J/m^3	$m^{-1} \cdot kg \cdot s^{-2}$
電界の強さ	ボルト毎メートル	V/m	$m \cdot kg \cdot s^{-3} \cdot A^{-1}$
体積電荷	クーロン毎立方メートル	C/m^3	$m^{-3} \cdot s \cdot A$
電気変位	クーロン毎平方メートル	C/m^2	$m^{-2} \cdot s \cdot A$
誘電率	ファラド毎メートル	F/m	$m^{-3} \cdot kg^{-1} \cdot s^4 \cdot A^2$
透磁率	ヘンリー毎メートル	H/m	$m \cdot kg \cdot s^{-2} \cdot A^{-2}$
モルエネルギー	ジュール毎モル	J/mol	$m^2 \cdot kg \cdot s^{-2} \cdot mol^{-1}$
モルエントロピー，モル熱容量	ジュール毎モル毎ケルビン	J/(mol・K)	$m^2 \cdot kg \cdot s^{-2} \cdot K^{-1} \cdot mol^{-1}$
照射線量（X線及びγ線）	クーロン毎キログラム	C/kg	$kg^{-1} \cdot s \cdot A$
吸収線量率	グレイ毎秒	Gy/s	$m^2 \cdot s^{-3}$
放射強度	ワット毎ステラジアン	W/sr	$m^4 \cdot m^{-2} \cdot kg \cdot s^{-3}=m^2 \cdot kg \cdot s^{-3}$
放射輝度	ワット毎平方メートル毎ステラジアン	$W/(m^2 \cdot sr)$	$m^2 \cdot m^{-2} \cdot kg \cdot s^{-3}=kg \cdot s^{-3}$

表６．国際単位系と併用されるが国際単位系に属さない単位

名称	記号	SI 単位による値
分	min	1 min=60s
時	h	1h =60 min=3600 s
日	d	1 d=24 h=86400 s
度	°	1°=(π/180) rad
分	’	1’=(1/60)°=(π/10800) rad
秒	”	1”=(1/60)’=(π/648000) rad
リットル	l、L	1l=1 $dm^3=10^{-3}m^3$
トン	t	1t=10^3 kg
ネーパ	Np	1Np=1
ベル	B	1B=(1/2)ln10(Np)

表７．国際単位系と併用されこれに属さない単位でSI単位で表される数値が実験的に得られるもの

名称	記号	SI 単位であらわされる数値
電子ボルト	eV	$1eV=1.60217733(49) \times 10^{-19}J$
統一原子質量単位	u	$1u=1.6605402(10) \times 10^{-27}kg$
天文単位	ua	$1ua=1.49597870691(30) \times 10^{11}m$

表８．国際単位系に属さないが国際単位系と併用されるその他の単位

名称	記号	SI 単位であらわされる数値
海里		1海里=1852m
ノット		1ノット=1海里毎時=(1852/3600)m/s
アール	a	1 a=1 $dam^2=10^2m^2$
ヘクタール	ha	1 ha=1 $hm^2=10^4m^2$
バール	bar	1 bar=0.1MPa=100kPa=1000hPa=10^5Pa
オングストローム	Å	1 Å=0.1nm=10^{-10}m
バーン	b	1 b=100$fm^2=10^{-28}m^2$

表９．固有の名称を含むCGS組立単位

名称	記号	SI 単位であらわされる数値
エルグ	erg	1 erg=10^{-7} J
ダイン	dyn	1 dyn=10^{-5}N
ポアズ	P	1 P=1 dyn・s/cm^2=0.1Pa・s
ストークス	St	1 St =$1cm^2/s=10^{-4}m^2/s$
ガウス	G	1 G ≙10^{-4}T
エルステッド	Oe	1 Oe ≙(1000/4π)A/m
マクスウェル	Mx	1 Mx ≙10^{-8}Wb
スチルブ	sb	1 sb =$1cd/cm^2=10^4cd/m^2$
ホト	ph	1 ph=10^4lx
ガル	Gal	$1 Gal =1cm/s^2=10^{-2}m/s^2$

表10．国際単位に属さないその他の単位の例

名称	記号	SI 単位であらわされる数値
キュリー	Ci	1 Ci=3.7×10^{10}Bq
レントゲン	R	1 R = 2.58×10^{-4}C/kg
ラド	rad	1 rad=1cGy=10^{-2}Gy
レム	rem	1 rem=1 cSv=10^{-2}Sv
X線単位		1X unit=1.002×10^{-4}nm
ガンマ	γ	1γ=1 nT=10^{-9}T
ジャンスキー	Jy	1 Jy=$10^{-26}W \cdot m^{-2} \cdot Hz^{-1}$
フェルミ		1 fermi=1 fm=10^{-15}m
メートル系カラット		1 metric carat = 200 mg = 2×10^{-4}kg
トル	Torr	1 Torr = (101 325/760) Pa
標準大気圧	atm	1 atm = 101 325 Pa
カロリー	cal	
ミクロン	μ	1 μ =1μm=10^{-6}m

（第７版，1998年改訂）